Investigation on the tensile strength, hardness and wear properties in n-B_4C reinforced Al7075 composites

M. Ravikumar
Dept., of Mechanical Engineering, B M S College of Engineering, Karnataka, India
ravikumarm.mech@bmsce.ac.in, https://orcid.org/0000-0002-4958-839X

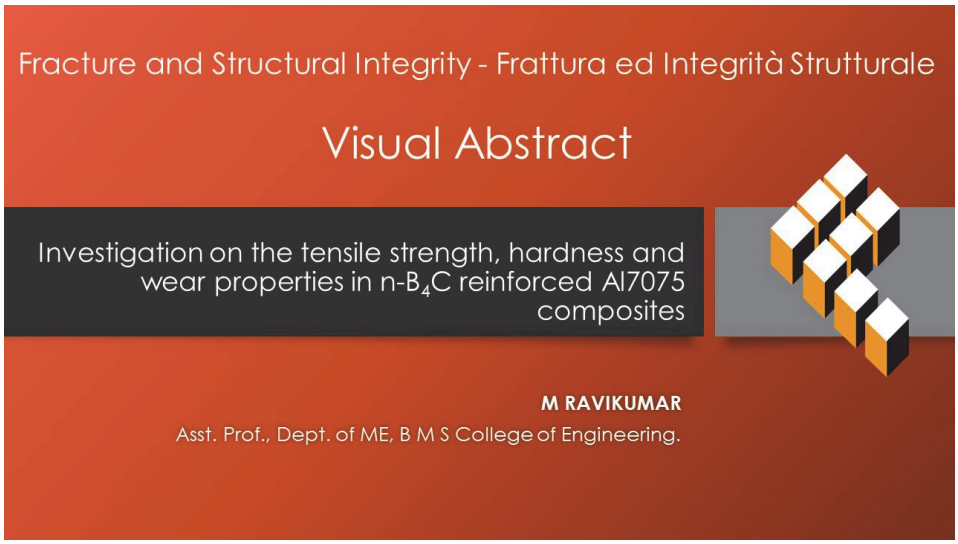

Citation: Ravikumar, M., Investigation on the tensile strength, hardness, and wear properties in n-B_4C reinforced Al7075 composites, Fracture and Structural integrity, 73 (2025) 219-235.

Received: 25.02.2025
Accepted: 10.04.2025
Published: 06.06.2025
Issue: 07.2025

KEYWORDS. Al7075, n-B_4C, Microstructure, Tensile strength, Hardness, Wear behavior, Fracture Surface.

INTRODUCTION

Metal matrix composites (MMCs) have several potential uses because of the distinct combination of characteristics that can be achieved. The demand for materials that possessed specific stiffness, durability, as well as wear resistance led to the development of MMCs. Aluminum is the perfect material for MMCs because of its low density, ease of manufacture, and advantageous technical characteristics. Al6061 and Al7075 are two heat-treatable alloys of aluminum that have been extensively studied. Because of its good corrosion resistance and moderate strength, Al6061 alloy finds extensive use in the construction, automotive, and marine industries. The automotive and aerospace industries appreciate Al7075 due of its outstanding tensile strength and enhanced toughness. MMCs may be produced by adding a reinforcement phase to the matrix. Suitable methods include squeeze casting, stir-casting, powder metallurgy, plasma spraying, spray atomization as well as co-deposition, and others. For the production of MMCs in engineered materials, casting is a unique approach due to its low cost, broad range of materials, and manufacturing conditions [1]. According to a review of the literature, the mechanical properties of stir-cast Al composites enhanced by

ceramic particulates have been extensively studied. Yu et al. [2] demonstrated the effects of temperature and applied load on the dry sliding wear characteristics of Al 6061-SiC composites and concluded that the wear rate decreased with increasing applied load. Pre-aging at various retrogation temperatures improves the hardness and tensile strength of Al7075, according to research by Reda et al. [3]. Straffelini [4] claim that the matrix hardness has a major impact on the dry sliding wear characteristics of Al 6061-Al_2O_3 composites. A unique physical mechanism mediates the wear process as per a study by Martin et al. [5] on the tribological properties of Al 6061-Al_2O_3 composites. SiC-reinforced Al 7075 was found by Doel and Bowen [6] to have less ductility and a higher tensile strength than unreinforced material. Al 7075-SiC composites offer superior mechanical properties, as demonstrated by Komai et al. [7]. Gudipudi et al. [8] investigated the effects of a special ultrasonic assisted stir-casting technique on the mechanical properties of AA6061-B_4C composites. Their results showed that at 4 weight percent B_4C, microstructure refinement and individual B_4C distribution were accomplished. The enhanced specific ultimate and compression strengths were 36.32% and 43.92% at 4 weight percent B_4C, while the specific Brinell as well as Vicker's hardness were 53.41% and 50.89%, respectively using microwave sintering, Jianhua Liu et al. [9] sated that, SiC as an reinforcements, generally enhanced the improvement in strength of aluminum metal matrix. SiC composites were reported to have a relative density about 96.14% and a hardness of 130 HV under ideal conditions, with Al/15 vol. %. The effects of two distinct alumina particle sizes on the wear and mechanical characteristics of the Al2024 alloy were investigated by M. Kok et al. [10]. They showed that the smaller particle reinforcement had a notably higher hardness and tensile strength than the larger particle size. The hardness and wear behavior of an Al6061 composite reinforced with three distinct SiC particles (19, 93, and 146) μm were examined by S. Mahdavi et al. [11]. According to their findings, the hardness increased as the SiC reinforcement's particle size decreased. As a result, it is noted that nothing is known about the mechanical and wear resistance of Al 7075 composites that have been augmented with particles. Prakash et al. [12] discussed the effect of hybrid reinforcements with different hardness (heat treatment) on mechanical and machinability characteristics of the developed hybrid composites. The result reveals that, the combined effect of hybrid reinforcements with heat treatment of wear loss of developed hybrid nano composites. The combined effect is not clear about on the indusial performance of the reinforcements, means Al_2O_3 is an oxides whereas B_4C is a carbide reinforcements. So, the microstructure and bonding strength of the reinforcements in the matrix is not clear. In the present research work, author focused on the effect of mono reinforcement (n-B_4C) on wear behavior of developed mono composites. Based on the above literature survey, it clearly states that, additions of nano ceramic reinforcements significantly influences the mechanical and wear properties. Therefore, in this work, Al7075/n-B_4C composites were processed via stir casting. The addition of nano particles to MMCs can significantly enhance the mechanical and wear properties. The incorporation of nano particulates, will helps to improve the bonding strength, hardness and also leds to high wear resistance. The novelty of the present work is to investigate the effect of n-B_4C reinforcements on tensile strength, hardness and wear properties in Al7075 MMCs. In the present study, detailed discussion on the microstructure, tensile fracture fractography and surface analysis of the developed n-B_4C reinforced Al7075 composites were studied and the wear parameters were optimized to evaluate wear rate of the developed nano composites.

MATERIALS AND METHOD

In the current investigation, stir casting was used to fabricate metal matrix composites using an Al7075 matrix reinforced with n-B_4Cp. Alloy Al7075 finds extensive use in Marine applications and aircraft structures. Tab. 1 shows the chemical composition of Al7075 in weight percentage. As reinforcements, particles with an average size of 40-60 nm were employed. The metal matrix composites were developed using the stir casting technique. During stirring process, the molten metal temperature was maintained at 680 °C. Further, the base alloy was combined with the pre-heated reinforced particles with temperature of 400 °C. The inert gases in the molten aluminum metal matrix were eliminated using degassing tablet. After five minutes of stirring at 100 rpm, the molten slurry was poured into a mold that was pre-heated. Cast samples were taken out of the mold once it had solidified. Computer numerical control (CNC) turning was used to pre-machine the samples. The samples were machined using coated carbide tool with cutting speed of 60 m/min, feed rate of 0.1 mm/rev and depth of cut of 0.2 mm. Diamond paste and 400 grit emery paper were used to polish the specimens' surfaces. To achieve a fine surface finish, the specimens were then polished using a velvet disc polishing equipment. Using a Nikon 200 optical metallurgical microscope, uniform distribution of reinforcement particulates in the matrix alloy was observed.

The Vickers hardness tester with a 10 mm diamond indenter was used to perform the micro hardness tests in accordance with ASTM E-92 requirements. Specimens were subjected to a load of 0.5 kg for 10 seconds. Average hardness value is

obtained by measuring the hardness at three separate points on the sample. In accordance with ASTM E8 specifications, tensile testing was performed using a 450 KN load on a Universal Testing Machine (UTM) (gauge length: 50 mm & gauge dia: 10 mm). Pin-on disc wear testing equipment was used to perform dry sliding wear tests as per ASTM with varying parameters, including weight percentage of nanosized B_4C particles (1%, 2%, and 3%), load of 7, 14, and 21 N, and sliding speed of 750, 1000, and 1250 rpm.

Content	Al	Cu	Mg	Si	Fe	Mn	Ni	Pb	Sn	Ti	Zn	Cr
wt. %	Rem	1.483	2.309	0.061	0.259	0.049	0.055	0.028	0.010	0.048	5.427	0.283

Table 1: Chemical Composition of Al7075 alloy with wt. %.

RESULTS AND DISCUSSION

Microstructural examination

The distribution of the reinforcing particles within the matrix material was investigated using microstructural analysis. The mechanical and tribological behaviors of Al7075/n-B_4C composites are governed by microstructural characteristics. Figs. 1(a) and (b) show the optical microstructure images of the basic matrix as well as composite reinforced with 3% n-B_4C. The fabricated nano composites samples' microstructural images display a homogeneous distribution of n-B_4C particulates with microscopic holes. Porosity could not be completely eliminated because the specimens were fabricated by stircasting. Microstructural images further show that cluster formation increases as the weight % of n-B_4C increases. The increased number of n-B_4C particulates is one of the primary reasons for the improved mechanical and tribological properties [13]. The consistent dispersion of n-B_4C particles within the matrix and the robust interfacial bond between the nano-particulates and the matrix are the primary causes of the enhanced mechanical and tribological characteristics of the n-B_4C composite. Grain structure can be changed by increased in n-B_4C particles since they can lead to an increase in nucleation sites and create more barriers to the spread of grain cracks.

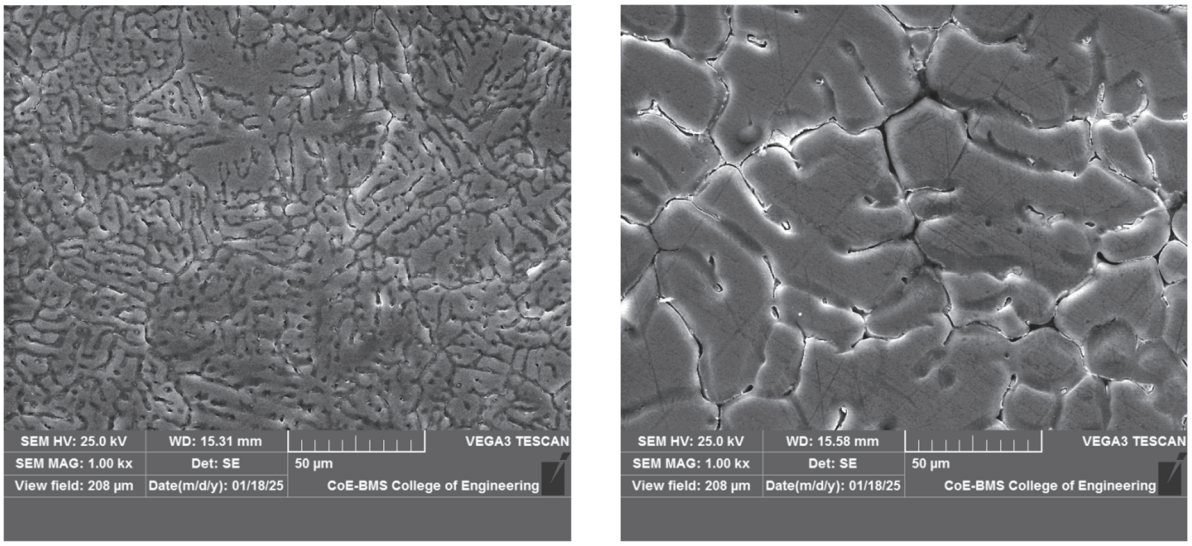

(a) (b)

Figure 1: Microstructure of the (a) matrix alloy (b) 3 wt.% n-B_4C reinforced composite.

Hardness

The hardness of a fabricated composite is determined by the hardness of the matrix phase and the reinforcing. Because nano-B_4C particles have a high hardness value, adding them should make the resulting composite harder. The results of the Vickers microhardness test are shown in Fig. 2. It shows that as the volume proportion of nano-B_4C reinforcement rises, so does the hardness. The quantity of additional reinforcement particles in composites determines the penetration depth. The reinforcing particle stops abrasion and distortion among mating surfaces by sustaining the generated contact stress. Addition of the n-B_4C reinforcement in MMCs is significantly affects hardness of the developed nano composites.

The hardness increases with 9.30 % for C2, 16.12 % for C3 and 17.89 % for C4 composites when compared to the pure aluminium alloy. The reason is that, particles can transfer load from the matrix, reducing the stress on the matrix and increasing the overall hardness in the developed nano composites (C1 – C3). Particles can acts as an obstacles to dislocation movements, increasing the strength and hardness of the develop nano composites. And also enhance the grain refinement in the composites. However, in the C4 composites shows the saturated hardness value of 95 VHN and it is very close to the hardness of C3 composites. It means that, the further increase of nano B_4C particulates leads to brittleness formation. It can conclude that, the increase in the wt. % of nano B_4C particles leads to increased hardness but, leds to decreased ductility.

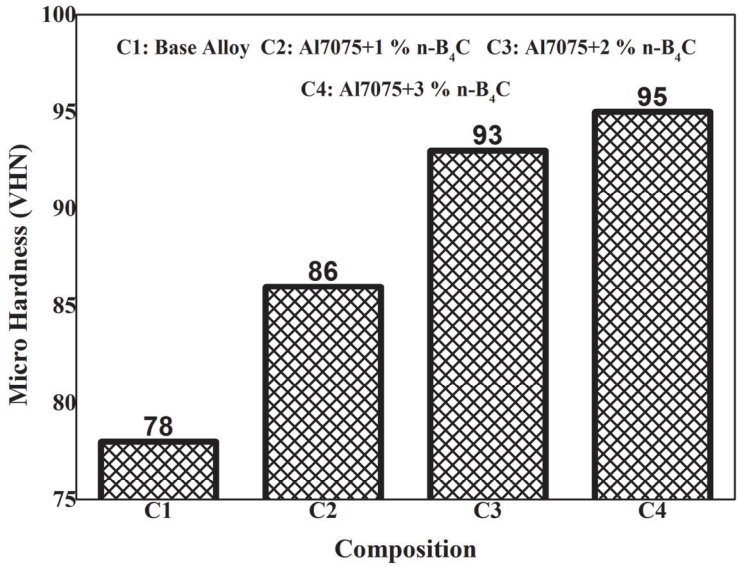

Figure 2: Vicker's micro hardness number for the base alloy and n-B_4C reinforced aluminium composites.

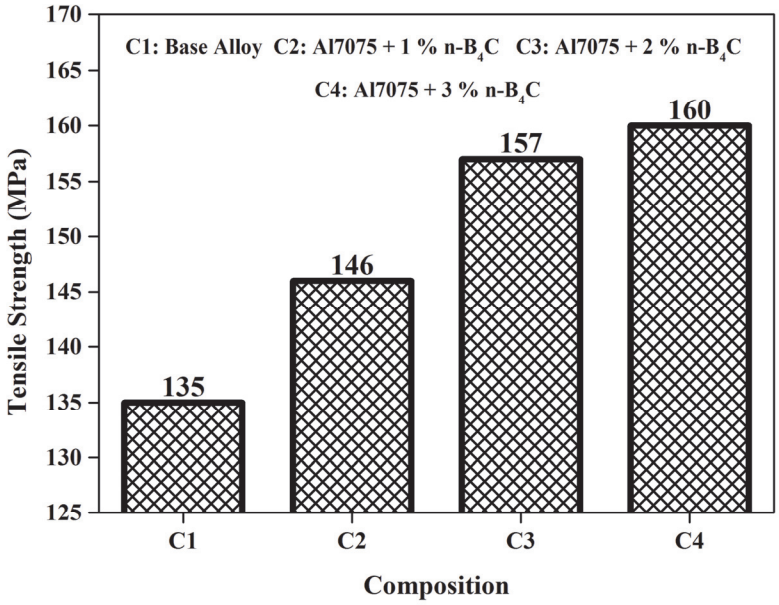

Figure 3: Tensile strength for the base alloy and n-B_4C reinforced aluminium composites.

Tensile strength

Microstructural alterations that affect mechanical qualities are prevented by expanding the amount of n-B_4C particulates in the developed composites. Fig. 3 displays the tensile characteristics of pure aluminum and n-B_4C reinforced aluminum network composites with 1, 2, and 3 weight percent n-B_4C particles. The strength (tensile) of all aluminum/n-B_4C composites is enhanced compared to the pure aluminum matrix, and it generally increases as the amount of n-B_4C

increases [13]. Both chemical bonding and mechanical anchoring are expected to produce the robust n-B_4C/aluminum bonding that is needed. Since an increasing concentration of nano-particulates represses matrix deformation in their region, it is envisaged that increasing silicon carbide fixation will result in an increase in stiff behavior conduct when compared to the relatively more flexible aluminum. At 3% addition, however, the characteristics barely change. Again, this has to do with the agglomeration phenomena. A poorer blending capacity brought on by the high viscosity in the particularly stacked composites is likely the cause of the voids and pores, which also influences the trend of the results [14]. It reveals that, effect of n-B_4C is increasing with increase of hardness and adverse effect on tensile strength and secondary process. It is due to the formation of brittleness formation of the composites with a higher probability of premature crack formation. Once reach the saturation of n-B_4C reinforcement in the matrix material, almost C3 and C4 composites resulted in small variation in the tensile strength. The tensile strength increases with 7.53 % for C2, 14.01 % for C3 and 15.62 % for C4 composites when compared to the pure aluminium alloy. Lower neck formation during tensile testing, the composite samples forming a smaller neck formation before fracture was observed. However, longer neck formation was occurred during the tensile testing of pure Al alloy.

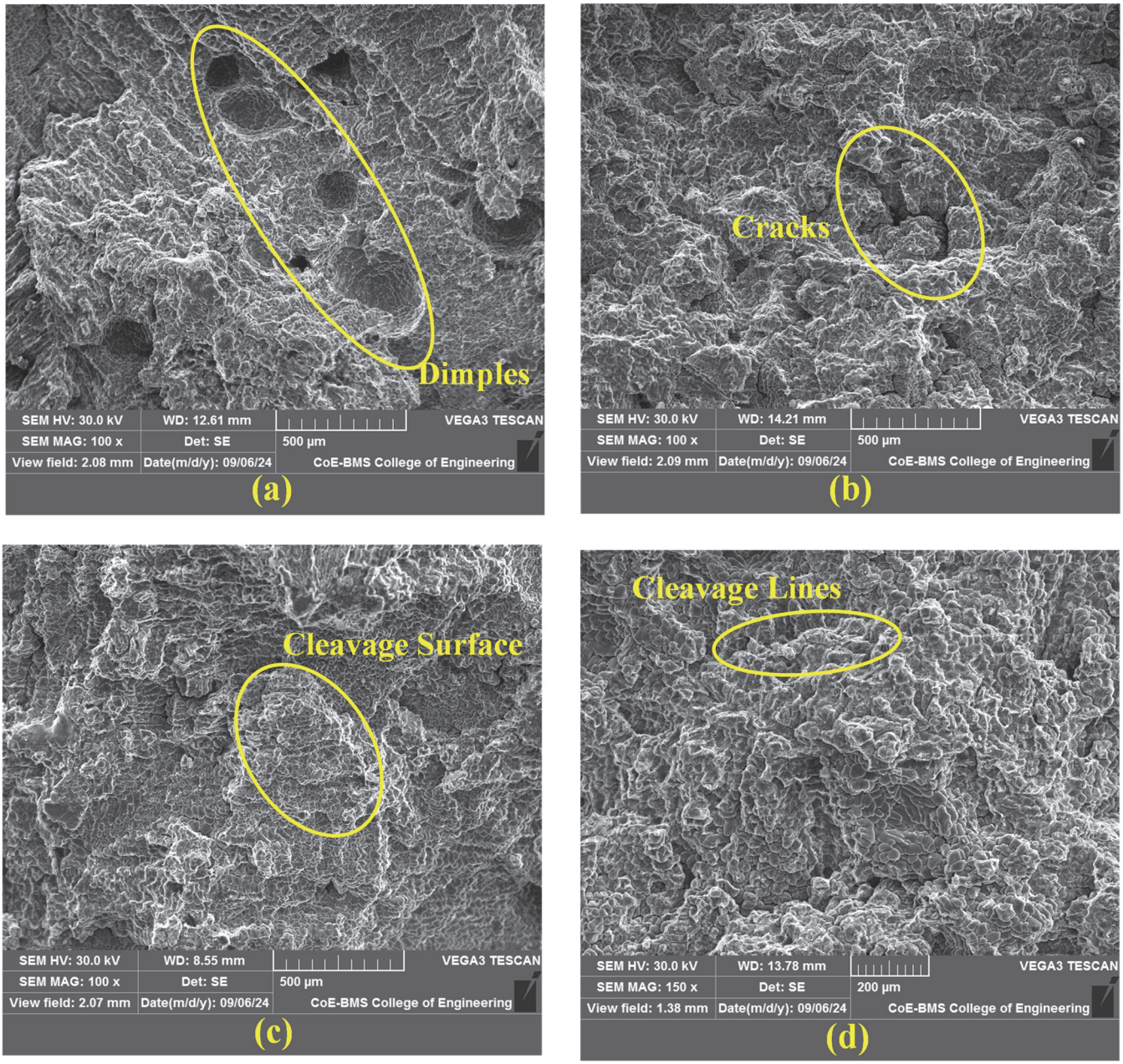

Figure 4: Fracture tensile surfaces for the (a) as-casted (b) 1 %, (c) 2 %, and (d) 3 % n-B_4C reinforced Al composites.

Fracture studies

SEM pictures of the fractured surfaces for both cast alloys and nano composites that underwent tensile testing were used to analyze the fracture processes (Fig. 4(a-d)). The ductile fracture mode of the Al7075 alloy as cast as shown in Fig. 4(a). It has no crack but huge number of dimple-shaped structures is observed. The fracture structures of 1, 2, and 3 weight percent n-B_4C reinforced MMCs show less ductile failure (Fig. 4(b-d)). It is commonly known that debonding at the interface among alumina particulates and the Al matrix alloy, matrix material fracture, and particle cracking can all result in MMC failure during tensile testing. Three weight percentages of n-B_4C composites' fracture surfaces revealed higher local stresses at the interfaces, which caused a break at the reinforcing particles. Comparable results were found in the study [15], which classified tensile fractures into two categories: brittle and ductile. The type of fracture on the fractured surface was determined by the intermetallic compounds that were produced and the irregular nano B_4C dispersion.

The aluminum matrix and nano-B_4C reinforcements have different load-carrying capacities due to the random reinforcement dispersion, which makes the synthesized material more vulnerable to crack initiation. Because of the necking phenomenon in the composites, a dimpled structure was seen on the fractured ductile surface. However, reduced deformation energies in brittle materials led to the establishment of cleavages and transgranular crack propagation. The dimples that appear in the unreinforced aluminum in Fig. 4(a) show that the materials have undergone plastic deformation, which causes a ductile fracture in the composite. On the cracked surface of the 1–3% nano-B_4C reinforced composite, minor cleavages were seen, indicating the composite's brittle failure as a result of the tougher B_4C reinforcements. The inclusion of B_4C reinforcements was observed to boost the cleavages' intensity. The inclusion of ceramic B_4C nanoparticles prevents the material from deforming plastically because the aluminum matrix and B_4C reinforcement have different CTEs, which causes cleavages on the cracked surface. When the applied load intensity exceeds the material's strength, the existence of transgranular cleavages in brittle materials accelerates the crack's transit through the grains and causes brittle fracture of the nano composite.

Wear behavior by design of experiments

The process of defining and analyzing every possible scenario, including different elements and variables that govern an inquiry, is known as Design of Experimentation, or DOE. Based on DOE, the Taguchi technique refines the response's most crucial parameter by combining theoretical and experimental methods. Here, three parameters (slide speed, applied load, and reinforcement weight percentage) with three design levels were used to examine the impact of control factors on wear loss as well as coefficient of friction, as indicated in Tab. 2. The degree of freedom is one less than the number of levels for each control parameter. The rule states that there should be at least one more experimental run for each control component and their interactions than there are degrees of freedom overall. As indicated in Tab. 3, the L27 orthogonal array was utilized with three factors and three-levels. Twenty-seven trials were conducted using the run order produced by the Taguchi model. Wear Loss as well as Coefficient of Friction were the model's answers. The arrangement of the columns in an orthogonal array was determined by the coefficient of friction, wear rate, percentage of reinforcing weight, sliding speed, and applied load. The model's goal was to lower the coefficient of friction and wear loss. Analysis of Variance (ANOVA) was performed on the results after the mean and SN ratios were determined.

Signal-to-Noise ratio analysis

Signal-to-Noise Ratio was examined using the "Smaller is better" hypothesis, similar analysis was observed in other researcher [1]. The delta value in Tabs. 4 and 5 represents a factor's influence. The difference between a factor's highest and lowest characteristics averages is known as the delta value. The delta value and the relevance of that parameter on the replies will both increase with the degree of variation. The rank of the parameter is determined by its relevance. The rank makes it evident that the wt. % of n-B_4C significantly affects the coefficient of friction as well as wear loss, which are subsequently influenced by the sliding speed and applied load.

Varying Parameters	Level - 1	Level - 2	Level - 3
n-B_4C (wt. %)	1	2	3
Load (N)	7	14	21
Sliding Speed (rpm)	750	1000	1250

Table 2: Control Parameters and their levels.

Sl. No.	n-B_4C (wt. %)	Load (N)	Sliding Speed (rpm)	Wear Loss (Grams)	COF (μ)
1	1	7	750	0.074	0.95
2	1	7	1000	0.086	0.92
3	1	7	1250	0.092	0.90
4	1	14	750	0.086	0.88
5	1	14	1000	0.094	0.84
6	1	14	1250	0.095	0.87
7	1	21	750	0.093	0.82
8	1	21	1000	0.090	0.80
9	1	21	1250	0.098	0.69
10	2	7	750	0.035	0.85
11	2	7	1000	0.074	0.78
12	2	7	1250	0.070	0.72
13	2	14	750	0.066	0.70
14	2	14	1000	0.068	0.69
15	2	14	1250	0.079	0.67
16	2	21	750	0.075	0.70
17	2	21	1000	0.088	0.68
18	2	21	1250	0.085	0.55
19	3	7	750	0.024	0.81
20	3	7	1000	0.025	0.60
21	3	7	1250	0.049	0.58
22	3	14	750	0.038	0.52
23	3	14	1000	0.046	0.55
24	3	14	1250	0.071	0.53
25	3	21	750	0.052	0.52
26	3	21	1000	0.060	0.56
27	3	21	1250	0.084	0.39

Table 3: L27 Orthogonal array of experimental layout.

Level	n-B_4C (wt. %)	Load (N)	Sliding Speed (rpm)
1	0.08978	0.05878	0.06033
2	0.07111	0.07144	0.07011
3	0.04989	0.08056	0.08033
Delta	0.03989	0.02178	0.02000
Rank	1	2	3

Table 4: Response Table for Wear Loss.

Level	n-B_4C (wt. %)	Load (N)	Sliding Speed (rpm)
1	0.8522	0.7900	0.7500
2	0.7044	0.6944	0.7133
3	0.5622	0.6344	0.6556
Delta	0.2900	0.1556	0.0944
Rank	1	2	3

Table 5: Response Table for COF.

Main Effects Plots for means

Following the DOE's implementation of MINITAB software, further analysis and main effect plots are plotted (Fig. 5 and 6). The optimal level of each control parameter was determined using S/N ratio charts. The major effects plot showed that a reinforcement of 3 wt. %, 7 N of applied load, and a sliding speed of 750 rpm produced the best results for the least amount of wear loss. Similarly, the main effects plot was used to determine the ideal level of processing variables for COF, 3 weight percent reinforcement, 21 N load, and 1250 rpm sliding speed. The wear and COF transition for various parameter values is displayed on the wear loss (Fig. 5) and COF (Fig. 6) graph. Wear loss for the fabricated nano composite increases as the applied load and sliding speed rise, but it decreases as the load increases. Likewise, for the created nan-composites, COF decreases as n-B_4C, applied force, and sliding speed rises.

Effect of varying parameters

Effect of n-B_4C (wt. %) on wear loss, Fig. 5 shows how the weight percentage n-B_4C affects the wear loss of the generated MMCs. As the percentage of n-B_4C content increases, the wear rate decreases because the hardness of the composites increases in proportion to the counter disc surface. The inclusion of n-B_4C reinforcement can improve the aluminum alloy's mechanical, microstructural, and physicochemical characteristics. Moreover, the number of dislocations and matrix deformation increased when n-B_4C particles were added to the matrix alloy [16].

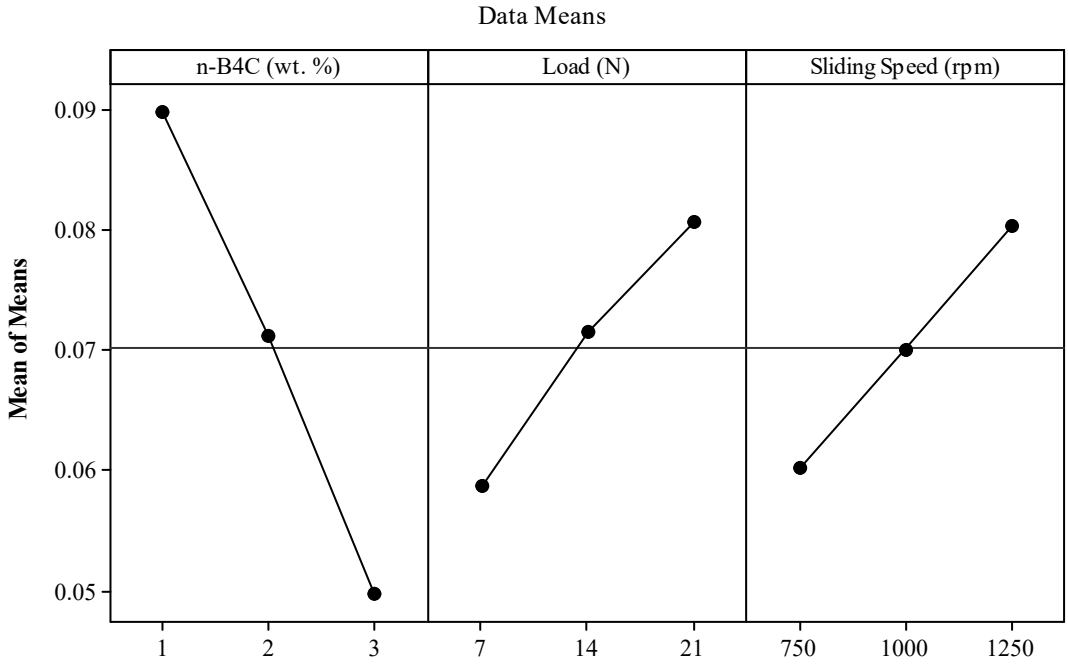

Figure 5: Main effects plots of wear loss.

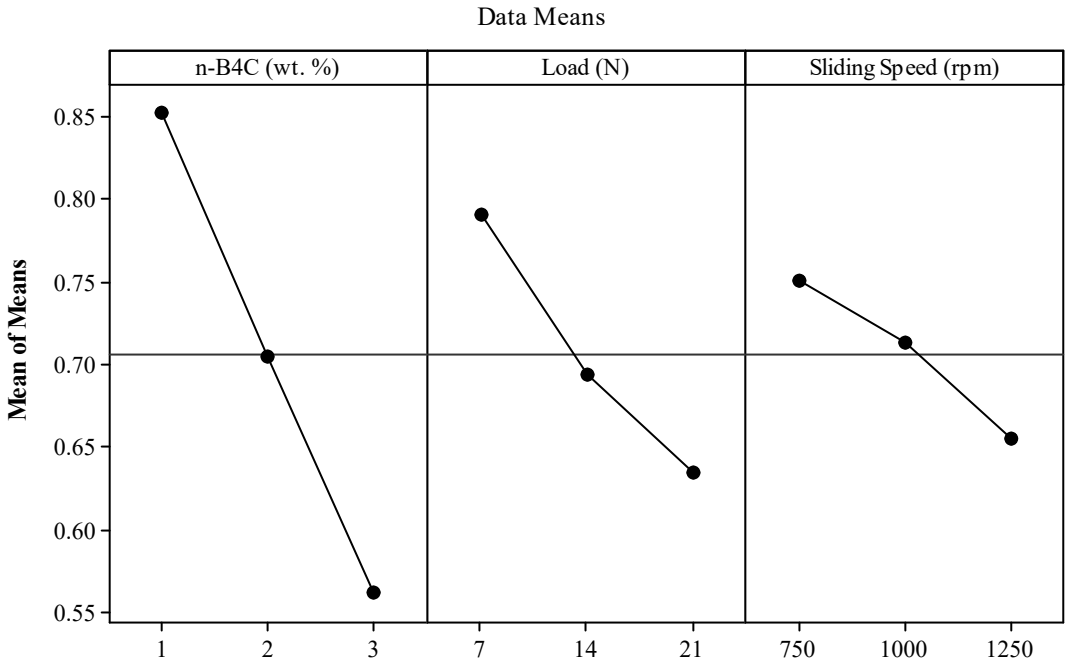

Figure 6: Main effects plots of COF.

Effect of load (N) on wear loss, Fig. 5 shows how load affects the wear loss of the generated nano composites. It is shown that the rate of wear first increases as the load increases. Later, when the load increases further, the pressure of contact among the tribo-pairs increases as well, this causes the additional weight to have a linear effect on the rate of increase. Less material is extracted from the interfaces because reduced loads result in less pressure being created. As a result, wear rates rose in proportion to an increase in applied load and material loss in the form of debris. Because of the larger deformation brought on by the produced high pressure between the interfaces, a higher rate of wear among the tribo-pairs is consequently observed under increased load [17].

Effect of sliding speed (rpm) on wear loss, it has been discovered that wear loss rises in tandem with sliding speed. Because the tribo pairs have greater opportunity to contact at lower sliding speeds, the interface temperature gradually rises, leading to oxidation. As a result, the tribo pairs undergo a material transformation. It promotes the formation of a mechanically mixed layer (MML) on the worn pin surfaces. By promoting further material loss from the surfaces, this phenomenon may lower wear rates. It is discovered that greater sliding speeds lead to reduced tribo-pair interaction, which in turn results in material transition and oxidation. There is a lower chance of MML production after this. Its amplification of tribo-pair interactions leads to higher wear rates [18].

Effect of n-B_4C (wt. %) on COF, Fig. 6 illustrates how the COF of the produced MMCs is impacted by the weight percentage n-B_4C. The use of extremely hard reinforced particles will lower the composite material's friction coefficient during the stable stage. Additionally, the decrease in the friction coefficient becomes more noticeable as the amount of additive increases. This is due to the fact that the contact area between the friction pair material and the matrix material is decreased during the friction process when reinforced particles are added to the matrix. This efficiently spreads the applied load and lowers the friction pair on the matrix material [19].

Effect of load (N) on COF, Fig. 6 illustrates how load (N) affects the produced nano composites' COF. It is discovered that there is an inverse relationship between the measured friction coefficient and the applied normal load, with the friction coefficient dropping as the normal load increases. Additionally, it was demonstrated that the wear rate was more affected by the load than the friction coefficient. Discs with a greater range of reinforcement experienced more friction, highlighting the clear influence of the reinforcement's size distribution once more. Furthermore, compared to its impact on wear behavior, the load had an inverse effect on the friction coefficient [17].

Effect of sliding speed (rpm) on COF, Fig. 6 illustrates how the COF of produced nano composites is impacted by sliding speed (rpm). As sliding speed increases, the friction factor decreases linearly due to the wettability among the base material and reinforcement particles [20, 21]. A change in the shear rate may be the cause of the drop in aluminum's friction coefficient as sliding speed rises, which may have an impact on the mechanical properties of the mating materials. A smaller actual area of contact and a lower coefficient of friction are the results of these materials' strength increasing with increasing shear strain rates under dry contact conditions.

Analysis of Variance (ANOVA)

To determine the importance of the factors and their interactions on both responses, an ANOVA was conducted at 95% confidence level and the 5% significant level (Tabs. 6 and 7). The amount of evidence needed in a sample to prove that the effect is statistically important and reject the null hypothesis is known as the significance level. If the "P" value probability, which gauges the evidence against the null hypothesis, is less than the importance threshold, as it is in this study, then rejecting it is supported; if not, it is supported. For wear loss and coefficient of friction, respectively, the final column in Tabs. 6 and 7 display the percentage significance of each metric. The wear rate is most affected by the wt. % of reinforcement (56.63%), which is followed by the load applied (16.88%) as well as sliding speed (14.23%), according to Tab. 6. Additionally, Tab. 7 demonstrates that the frictional coefficient is most affected by the weight percentage of reinforcement (65.60%), followed by load (18.87%) as well as sliding speed (6.95%). The percentage of significance of each metrics analysis was done using ANOVA analysis. The percentage of contribution was calculated using the following Eqn. 1,

$$\% \text{ of cont.} = (\text{Each Seq. SS} / \text{Total Seq. SS}) * 100 \quad (1)$$

Sources	DoF	Seq. SS	Adj. SS	Adj. MS	F - Value	P - Value	% of Cont.
n-B_4C (wt. %)	1	0.0071601	0.0071601	0.0071601	106.321	0.0000000	56.63
Load (N)	1	0.0021342	0.0021342	0.0021342	31.691	0.0000099	16.88
Sliding Speed (rpm)	1	0.0018000	0.0018000	0.0018000	26.729	0.0000306	14.23
Error	23	0.0015489	0.0015489	0.0000673			12.25
Total	26	0.0126432					99.99

Table 6: ANOVA results of wear loss.

Sources	DoF	Seq. SS	Adj. SS	Adj. MS	F - Value	P - Value	% of Cont.
n-B_4C (wt. %)	1	0.378450	0.378450	0.378450	176.373	0.0000000	65.60
Load (N)	1	0.108889	0.108889	0.108889	50.747	0.0000003	18.87
Sliding Speed (rpm)	1	0.040139	0.040139	0.040139	18.706	0.0002504	6.95
Error	23	0.049352	0.049352	0.002146			8.55
Total	26	0.576830					99.97

Table 7: ANOVA results of COF.

Interaction effects of parameters and residuals plots

ANOVA was used to assess the correlations between the three process parameters weight percentage of reinforcement, load applied, and sliding speed. The interaction plot matrix of numerous process parameters on hardness and wear loss is clearly shown in Figs. 7 and 8. For ease of reading, this graph displays the interaction effects for three distinct parameters: weight percentage of reinforcement, applied load, and sliding speed. If the interaction lines in the plots are parallel to the other parameter lines, then there is no interaction between the parameters. On the other hand, it signifies that the parameters are interacting when lines in a plot actually cross one another. The parameters employed in the study typically have an impact on the interaction's outcomes. The influence of wear parameters is typically shown by the interaction plots (graphs). According to the findings of other studies [22], the process parameter with the highest inclination line was more significant. It is determined that there is a better interaction between the parameters if the lines in the interaction graphs are not parallel. It is evident from the wear loss and COF interaction graph that the lines are not intersecting between the parameters. Therefore, the interaction effect is insignificant in wear loss and COF interaction graphs.

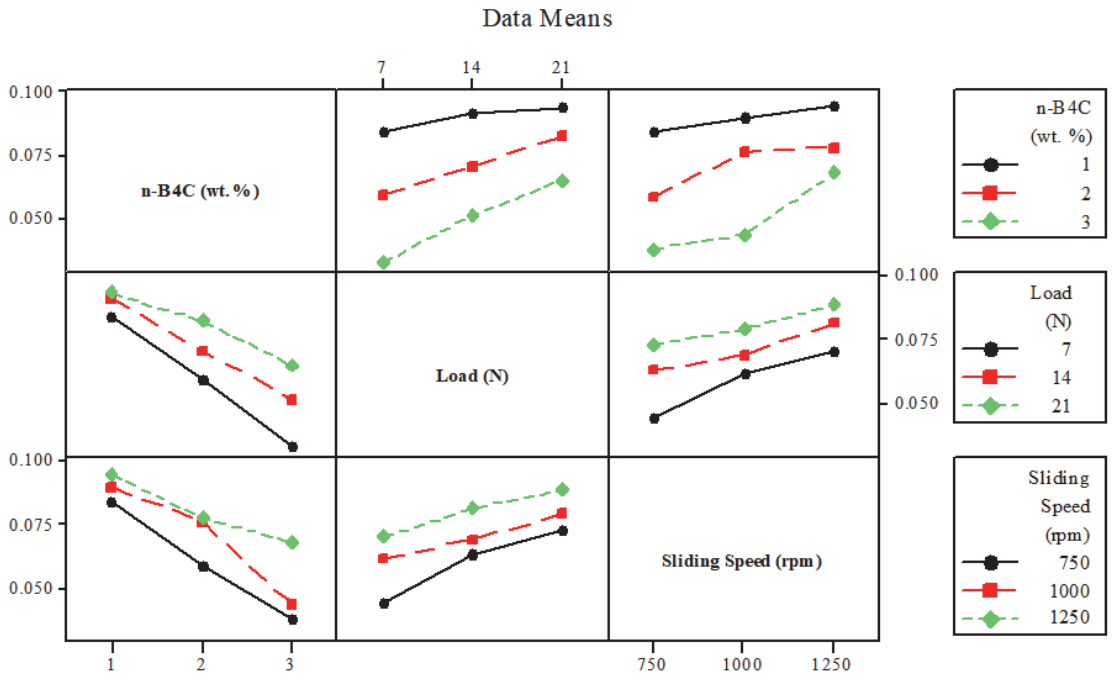

Figure 7: Interactions plot of Wear loss.

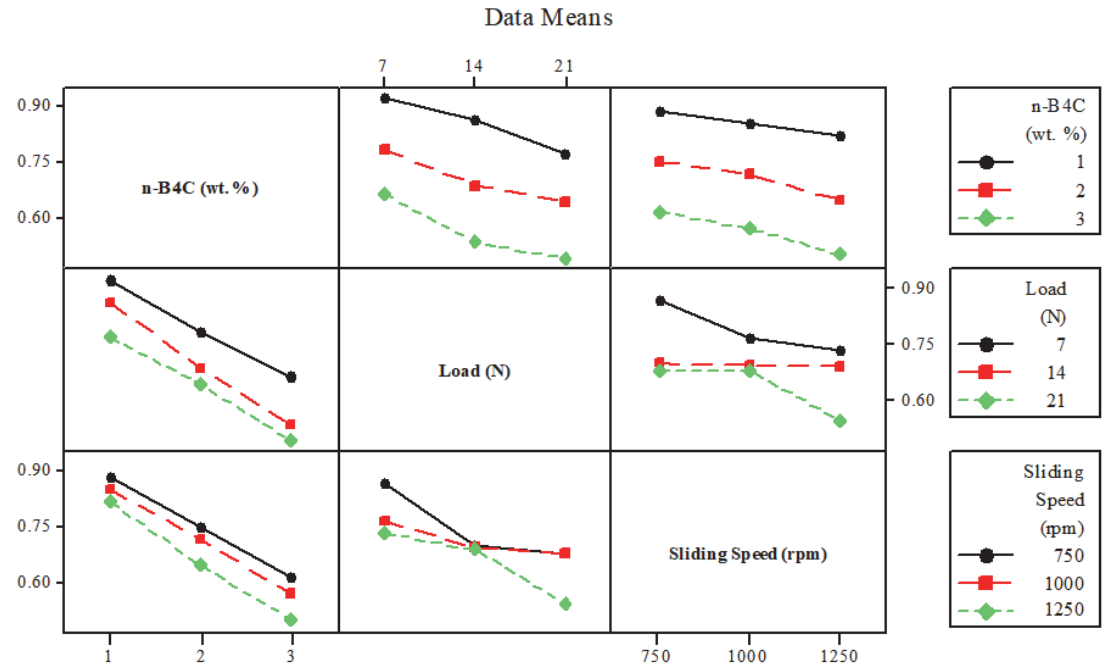

Figure 8: Interactions plot of COF.

Figs. 9 and 10 show the normal probability plots for wear loss and COF reveal errors that are uniformly distributed and have residuals that lie inside a straight line. This implies that the residuals are more uniformly distributed and have a better fit. In the meanwhile, the points are allegedly close to a straight line, and the collected data indicates no deviation. A non-linear relationship is typically indicated by the random pattern seen in the residual vs. fitted value charts. The residuals plots show that neither side of the zero line on the residual v/s. order plot shows clear pattern that would suggest a significant influence on the order of data collection. It is also shown that the residual points on either side of the zero line are evenly spaced, which often indicates that the residual density is about the same. The standardized residual histogram plot in this investigation exhibits little skewness and no outliers. Furthermore, residuals from the minimum to maximum range are displayed in the data, demonstrating the high accuracy of the conclusions [23].

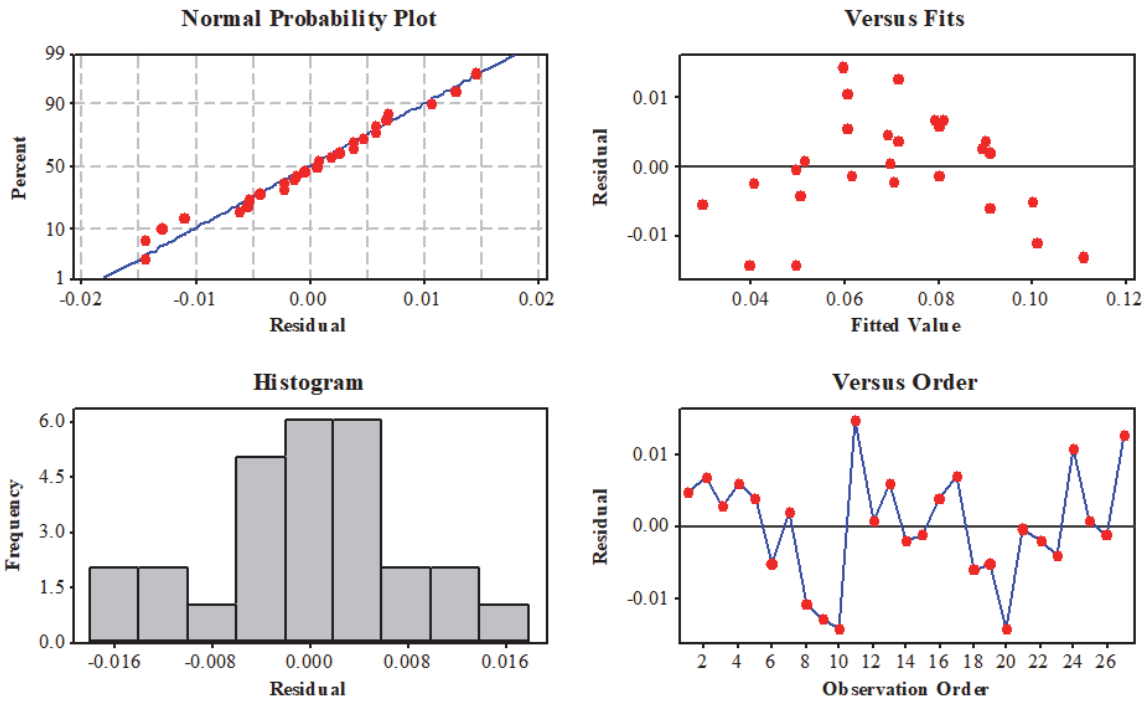

Figure 9: Residual plots of wear loss (grams).

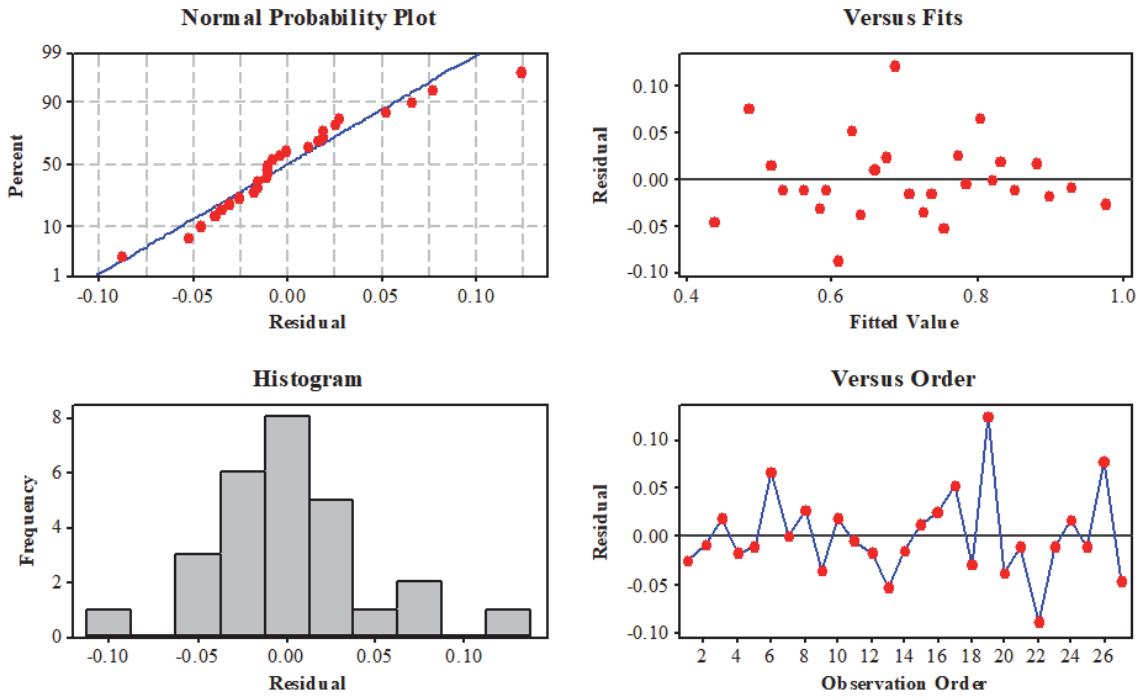

Figure 10: Residual plots of COF (μ).

Regression analysis

The regression models have shown a correlation between the answers and specific process variables, including the weight percentage of reinforcement (n-B_4C), applied load, and sliding speed. The regression equations are constructed using the significance of the parameters obtained from the ANOVA. The generated model's suitability for both responses is confirmed by the validation exercise. After modifying the built model to include the anticipated sets of process variables, the response obtained for both outputs is contrasted with experimental values obtained for the same set of parameters. The relevant equations for regression for both are given in Eqns. 2 and 3 below.

$$\text{Wear Loss (g)} = 0.0483704 - 0.0199444\ (\text{n-B}_4\text{C}) + 0.00155556\ (\text{Load}) + 4\text{e-}005\ \text{Sliding Speed} \quad (2)$$

$$\text{COF } (\mu) = 1.34074 - 0.145\ (\text{n-B}_4\text{C}) - 0.0111111\ (\text{Load}) - 0.000188889\ (\text{Sliding Speed}) \quad (3)$$

Generally speaking, these equations (regression) have been used to estimate the responses within the parameters. Graphical comparisons between the predicted and experimental results have been created, and experiments have been carried out to confirm the prediction values' correctness. Comparison of the predicted and experimental values for COF and wear loss is shown in Fig. 11(a) and (b), respectively. The plots demonstrate that the expected and experimental values have a strong relationship.

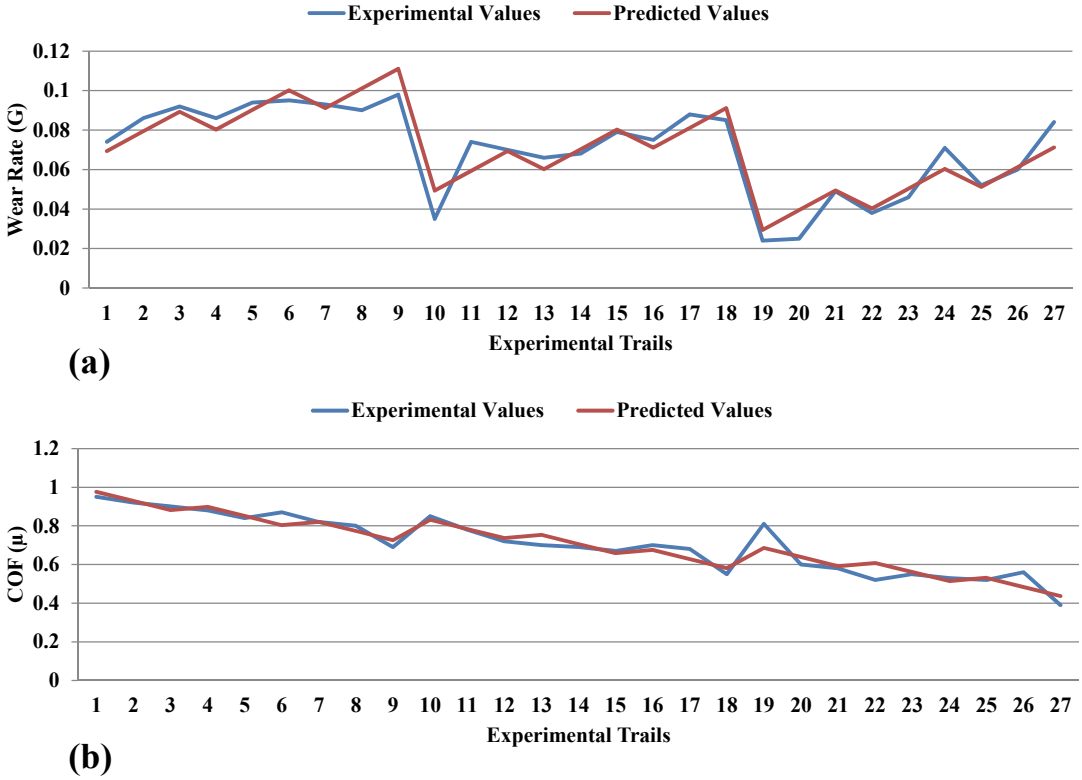

Figure 11: Comparison response of experimental values with predicted values for (a) wear loss and (b) COF.

Confirmation experiments

The experiment design process was completed with a confirmation test. For the ideal parametric settings recommended by the genetic algorithm and Taguchi method, confirmation experiments were carried out. The optimal parameter settings were found using the Main Effects Plot for Means. This was within reasonable limitations, as can be seen. The wear test findings indicated a maximum of 4.166% error, while the confirmatory test results showed a maximum of 5.128% errors/deviation in the COF of nano composites. Tab. 8 displays the ideal-level values for conducting confirmation tests as well as the response of confirmation tests.

Exp. Sources	Process Parameters			OA Exp. Outcomes	Confirmatory Exp. Outcomes	Error (%)
	n-B_4C (wt. %)	Load (N)	Sliding Speed (rpm)			
Wear Loss (g)	3	7	750	0.024	0.025	4.166
COF (μ)	3	21	1250	0.39	0.041	5.128

Table 8: Confirmation test results.

SEM analysis of wornout surfaces

The SEM micrographs of the Al7075 alloy and Al+n-B_4C wear tracks are shown in Fig. 12 (a-d). The SEM images clearly show the wear traces and the direction of wears. Narrow wear grooves and a few microcracks are visible in the darker layer which represents the wear traces. Additionally, compared to pure samples, wear traces are more pronounced for composites enhanced with nanoparticles (Fig. 12 (b-d)). Significant flash temperatures produced at the contact surface over long distances result in a noticeable scorched patch, as seen in Fig. 12 (b-d). Examples of how wear debris produced during sliding functions as abrasive particles and speeds up abrasive wear and removal of material from the surface include plowing and pit creation.

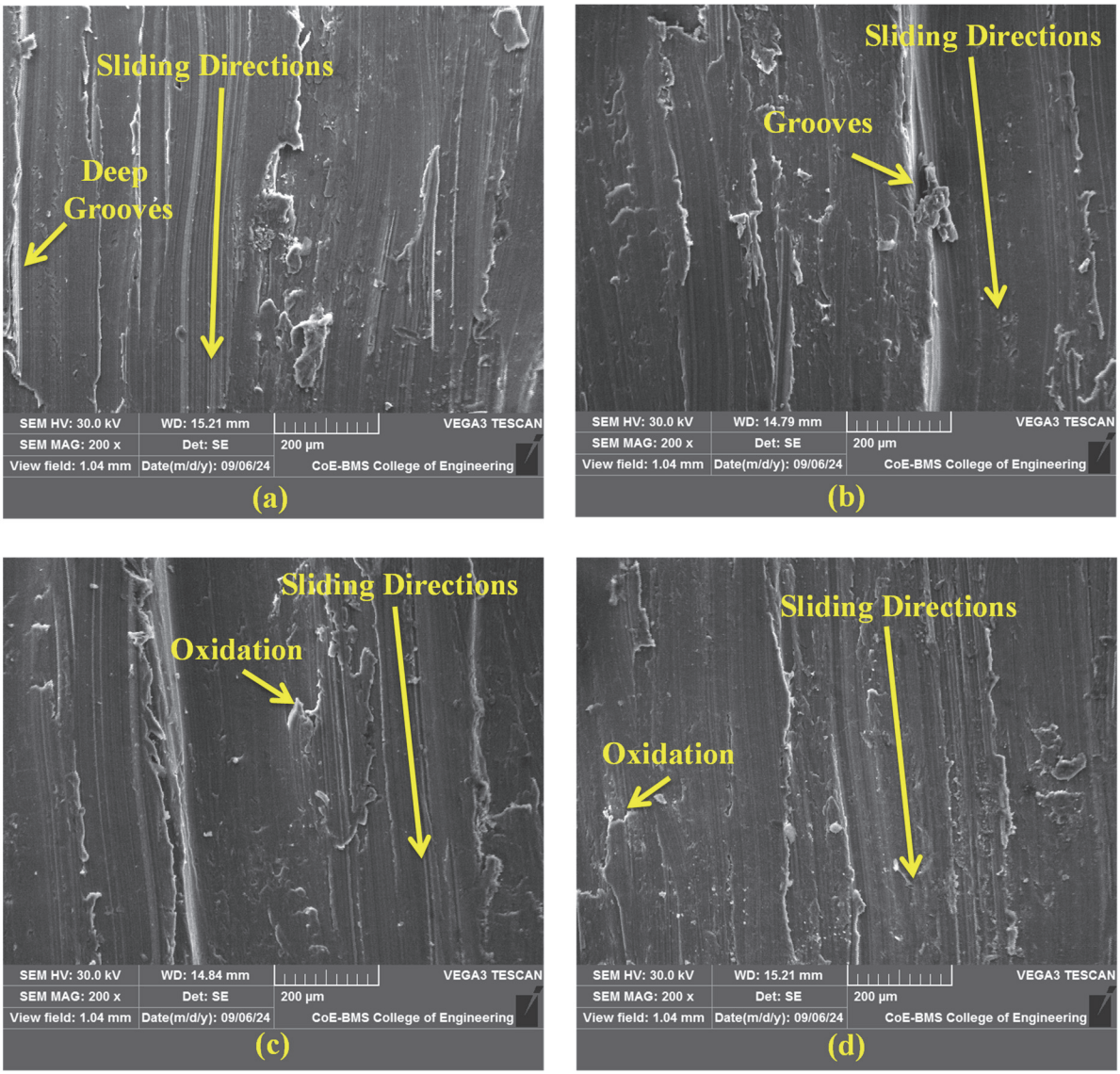

Figure 12: Wornout surfaces for the (a) as-casted (b) 1 wt. %, (c) 2 wt. %, and (d) 3 wt. % n-B_4C reinforced Al composites.

Every worn micrograph displays groove markings that are caused by reinforcing particles rubbing against one another in the sliding direction. These findings suggest that a mechanically mixed layer (MML) has developed in the darker regions of the worn surface as a result of material transfer and mechanical mixing between the two sliding surfaces. Therefore, in the case of produced nano composites, wear resistance appears to have been caused by a mechanical mixing with oxidation process. The worn-out surface of Al7075+n-B_4C shows how the n-B_4C particles in Al7075 restrict the matrix's viscous flow, which reduces erosion or grooves and, as a result, increases wear resistance. As the number of n-B_4C particles rises, worn areas show less and fewer cracks and grooves, indicating that stress is focused on and transferred to these particles [24].

Energy Dispersive spectrum (EDS) Analysis

EDS provides qualitative and semi-quantitative information on the composition of a sample and is especially helpful for identifying materials on its surface. Fig. 13 (a) displays the aluminum alloy's EDS spectrum. It suggests the existence of a substantial amount of aluminum together with elements like Zn, Mg, Fe, Mn, and Cu. Fig. 13(b) displays the EDS spectra of a nano composite sample that contains 3% nanosized B_4C. In addition to Al and Zn, it is seen that the Al-7075 alloy matrix includes nano B_4C particulates in the form of B and C constituents [25].

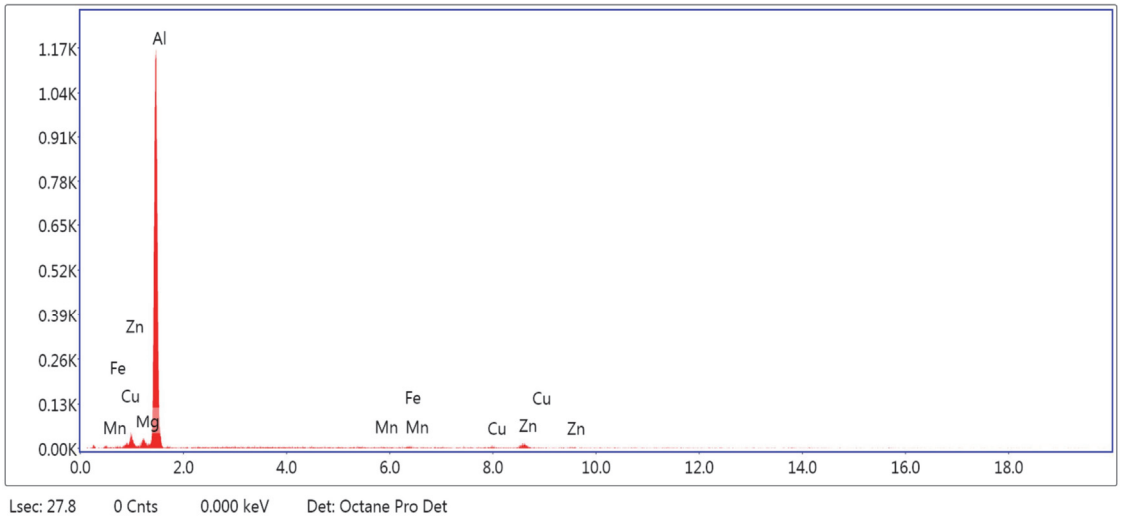

(a)

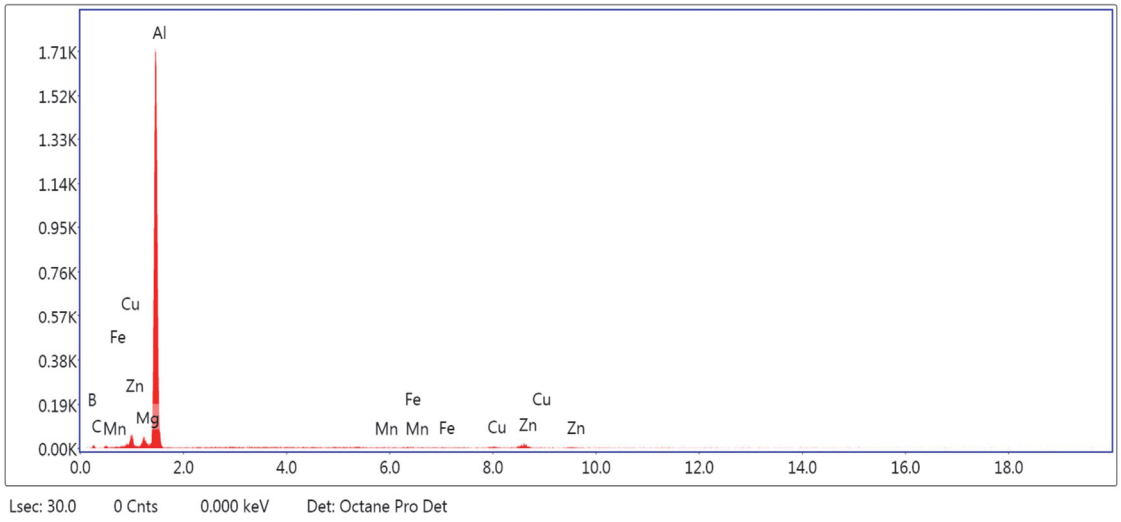

(b)

Figure 13: EDS spectrums of (a) base alloy (Al7075) and (b) Al7075-3 wt. % n-B_4C composites.

CONCLUSIONS

- Stir casting has been shown to be a successful technique for fabricating Al7075 alloy composites reinforced with 1%–3% nanosized B_4C particles.
- The findings of the microstructural studies showed that the nanosized B_4C was uniformly distributed throughout the aluminum matrix.
- The hardness increases with 9.30 % for C2, 16.12 % for C3 and 17.89 % for C4 composites when compared to the pure aluminium alloy.

- When n-B_4C particles were introduced to the Al7075 matrix, the material's tensile strength increased. The composite's ultimate strength rose from 135 MPa to 160 MPa when 3 wt. % of nanosized B_4C nanoparticles was added to Al7075.
- When the intensity of the applied load exceeded the strength of the material, the existence of transgranular cleavages increased the crack's ability to propagate across the grains and caused brittle fracture of the nano composite, as the broken surface illustrates.
- The wear characteristics of Al7075 and its nano composites were discovered to be influenced by the weight percentage of n-B_4C, the applied load, and the sliding speed. The frequency of cracks and grooves in worn areas decreased as the quantity of n-B_4C particles increases, indicating that stress is transferred to and centered on these particles. However, nano B_4C composites with weight proportions of 1, 2, and 3 greatly increased the wear resistance.
- Energy dispersive spectrum (EDS) measurement confirmed the existence of nano B_4C particles in the Al7075 alloy matrix within the form of B and C elements in addition to Al and Zn.

REFERENCES

[1] Sreenivasa Iyengar, S.R., Sethuramu, D., and Ravikumar, M. (2023). Study on hardness, fracture behavior and optimization of wear characteristics of Al6061/TiB_2/CeO_2 MMCs using Taguchi method, Frattura ed Integrità Strutturale, 64, pp. 178-193.

[2] Yu, S. H., Ishii, H., Tohgo, K., Cho, Y. T. and Diao, D. (1997). Temperature dependence of sliding wear behavior in SiC whisker or SiC particulate reinforced 6061 aluminum alloy composite. Wear, 213, pp. 21-8.

[3] Reda, Y., Abdel-Karim, R., and Elmahallawi, I. (2008). Improvements in mechanical and stress corrosion cracking properties in Al-alloy 7075 via retrogression and re-aging. Material Science Engineering - A, 485(1-2), pp. 468-75.

[4] Straffelini, G., Bonollo, F., and Tiziani, A. (1997). Influence of matrix hardness on the sliding behavior of 20 vol% Al_2O_3-particulate reinforced 6061 Al metal matrix composite. Wear, 211, pp. 192-7.

[5] Martin, J., Rodriguez, J., and Llorca, J. (1999). Temperature effects on the wear behavior of particulate reinforced Al-based composites. Wear, pp. 225-229.

[6] Doel, T. J. A., and Bowen, P. (1996). Tensile properties of particulate-reinforced metal matrix composites. Composites Part A: Applied Science and Manufacturing, 27(8), pp. 655-65.

[7] Komai, K., Minoshima, K., and Ryoson, H. (1993). Tensile and fatigue fracture behavior and water-environment effects in a SiC-whisker/7075-aluminum composite. Composites Science and Technology, 46(1), pp. 59-66.

[8] Gudipudi, S., Nagamuthu, S., Subbian, K. S., Prakasa, S., and Chilakalapalli, R. (2020). Enhanced mechanical properties of AA6061-B_4C composites developed by a novel ultra-sonic assisted stir casting. Engineering Science and Technology, an International Journal, 23, pp. 1233-1243.

[9] Iqbal, A. A., Lim, M. J., and Nuruzzaman, D. M. (2017). Effect of compaction load and sintering temperature on the mechanical properties of the Al-SiC nano-composite materials. AIP Conference Proceedings, pp. 1-8. DOI: 10. 1063/1. 50104 71.

[10] Kok, M., and Ozdin, K. (2007). Wear resistance of aluminium alloy and its composites reinforced by Al_2O_3 particles. Journal of Materials Processing Technology, 183, pp. 301-309, DOI: 10.1016/j.jmatprotec.2006.10.021.

[11] Mahdavi, S. and Akhlaghi, F. (2011). Effect of the SiC particle size on the dry sliding wear behavior of SiC and SiC-Gr-reinforced Al6061 composites. Journal of Materials Science, 46, pp. 7883-7894, DOI:10.1007/s10853-011-5776-1.

[12] Prakash, T.B., Gangadharappa, M., Santhosh, S. and Ravikumar, M. (2024). Impact of nanoparticles (B_4C-Al_2O_3) on mechanical, wear, fracture behavior and machining properties of formwork grade Al7075 composites, Frattura ed Integrità Strutturale, 69, pp. 210-226.

[13] Jong, S. C. (2013). Recent progress in the development and properties of novel metal matrix nanocomposites reinforced with carbon nanotubes and graphene nano sheets. Materials Science and Engineering: R: Reports, 74, pp. 281-350.

[14] Faisal, N. and Kumar, K. (2018). Mechanical and tribological behaviour of nano scaled silicon carbide reinforced aluminium Composites. Journal of Experimental Nanoscience, 13, DOI: 10.1080/17458080.2018.1431846.

[15] Venkatesh, V. S. S., Rao, G. P., Patnaik, L., Gupta, N., Kumar, S., Saxena, K. K., Sunil, B. D. Y., Sayed, M. E. and Al kafaji, F. H. K. (2023). Processing and evaluation of nano SiC reinforced aluminium composite synthesized through ultrasonically assisted stir casting process. Journal of Material Research and Technology, 24, pp. 7394-7408.

[16] Wang, Y. and Zhang, J. (2023). A review of the friction and wear behavior of particle-reinforced aluminum matrix composites. Lubricants, 11 (8), DOI: 10.3390/lubricants11080317.

[17] Khan, M. M., Dey, A. and Hajam, M. I. (2022). Experimental Investigation and Optimization of Dry Sliding Wear Test Parameters of Aluminum Based Composites. Silicon, 14, pp. 4009-4026. DOI: 10.1007/s12633-021-01158-5.

[18] Zhang, J. and Alpas, A. T. (1997) Transition between mild and severe wear in aluminium alloys. Acta Materialia, 45(2), pp. 513-528.

[19] Uyyuru, R. K., Surappa, M. K., and Brusethaug, S. (2007). Tribological behavior of Al-Si-SiCp composites/automobile brake pad system under dry sliding conditions. Tribology International, 40, pp. 365-373.

[20] Nisar, A., Khan, M. M., Bajpai, S. and Balani, K. (2019). Processing, microstructure and mechanical properties of HfB_2-ZrB_2-SiC composites: Effect of B_4C and carbon nanotube reinforcements. International Journal of Refractory Metals and Hard Materials, 81, pp. 111-118.

[21] Daniel, A. A., Murugesan., Manojkumar and Sukkasamy, S. (2017). Dry Sliding Wear Behaviour of Aluminium 5059/SiC/MoS_2 Hybrid Metal Matrix Composites. Materials Research, 20(6), pp. 1697-1706.

[22] Shaikh, M. B. N. (2018). A statistical analysis of wear behaviour of fly ash reinforced Al-SiC hybrid composites. Journal of Powder Metallurgy & Mining, 7(1), pp. 190-194. DOI:10.4172/2168-9806.1000190.

[23] Sesharao, Y., Sathish, T., Palani, K., Merneedi, A., Natrayan, L., Depoures, M. V. and Thirupathy, M. (2021). Optimization on Operation Parameters in Reinforced Metal Matrix of AA6066 Composite with HSS and Cu, Advances in Materials Science and Engineering, DOI: 10.1155/2021/1609769.

[24] Ravindra, Rajesh, M., Kumar, K. D., Sailender, M., Pathalinga Prasad, G., Nagaraj, N. and Ramulu, P. J. (2023). Effect of Boron Carbide Particles Addition on the Mechanical and Wear Behavior of Aluminium Alloy Composites. Advances in Materials Science and Engineering, DOI: 10.1155/2023/2386558.

[25] Suresh, B. S., Manjunath, S. H., and Girish, K. B. (2023). Characterization of Aluminium Alloy LM6 with B_4C and Graphite Reinforced Hybrid Metal Matrix Composites. Engineering Proceedings, 59(72), pp. 1-13, DOI: 10.3390/engproc2023059072.